DETECTION OF 55–80 keV HYDROGEN ATOMS OF HELIOSPHERIC ORIGIN BY CELIAS/HSTOF ON *SOHO*

M. HILCHENBACH,[1] K. C. HSIEH,[2] D. HOVESTADT,[3] B. KLECKER,[3] H. GRÜNWALDT,[1] P. BOCHSLER,[4] F. M. IPAVICH,[5]
A. BÜRGI,[6] E. MÖBIUS,[7] F. GLIEM,[8] W. I. AXFORD,[1] H. BALSIGER,[4] W. BORNEMANN,[3] M. A. COPLAN,[5]
A. B. GALVIN,[7] J. GEISS,[9] G. GLOECKLER,[5] S. HEFTI,[4] D. L. JUDGE,[10] R. KALLENBACH,[9]
P. LAEVERENZ,[3] M. A. LEE,[7] S. LIVI,[1] G. G. MANAGADZE,[11] E. MARSCH,[1]
M. NEUGEBAUER,[12] H. S. OGAWA,[10] K.-U. REICHE,[8] M. SCHOLER,[3]
M. I. VERIGIN,[11] B. WILKEN,[1] AND P. WURZ[4]

ABSTRACT

The High-Energy Suprathermal Time-of-Flight sensor (HSTOF) of the Charge, Element, and Isotope Analysis System (CELIAS) on the *Solar and Heliospheric Observatory* (*SOHO*) near the Lagrangian point L1 is capable of identifying energetic hydrogen atoms (EHAs) between 55 and 80 keV. Between 1996 February 13 and 1997 August 31, near solar minimum, there were 285 "quiet" days when the interplanetary charged-particle flux was low. During these quiet times, HSTOF scanned the apex of the heliosphere once and the antiapex twice. The flux level and time profile, and hence the arrival direction, of the EHAs accumulated during these quiet times are best interpreted as fluxes of EHAs coming from the heliosheath.

Subject headings: cosmic rays — ISM: atoms — solar wind

1. INTRODUCTION

It was recognized in the early 1990s (Hsieh et al. 1992a, hereafter H1) that the detection of energetic neutral atoms (ENAs) of heliospheric origin could provide a unique channel, independent of the interplanetary magnetic field, to study the acceleration and propagation of charged particles, especially the anomalous cosmic rays (ACRs), in and out of the heliosphere. The potential utility of ENAs in the investigation of ions at a distance promoted further studies (Hsieh et al. 1992b, hereafter H2; Roelof 1992; Hsieh & Gruntman 1993; Czechowski, Grzedzielski, & Mostafa 1995, hereafter CGM). The first opportunity to detect ENAs of heliospheric origin came with the High-Energy Suprathermal Time-of-Flight sensor (HSTOF) of the Charge, Element, and Isotope Analysis System sensor (CELIAS) (Hovestadt et al. 1995) on *SOHO* (Fleck, Domingo, & Poland 1995), launched during solar minimum on 1995 December 2. We report here the first likely detection of energetic neutral atoms of heliospheric origin.

An ENA starts as an energetic +1 ion, before picking up an electron from a neutral atom of the ambient gas. Charge transfers occur at internuclear distances of atomic scale, so that each ENA effectively retains its original energy. Being neutral, ENAs are unaffected by magnetic fields, so each ENA preserves the direction of flight at its birth, moving along a ballistic trajectory to distant regions unreachable by the original population of ions. Thus, ENAs are samples of remote space plasmas inaccessible to in situ observations of ions. The shape of an ENA energy spectrum is formed by the product of the original ion spectrum and the sum of charge-exchange cross sections, weighted by the number densities of the respective neutral atoms in the ambient gas. Since the ion fluxes of most varieties of space plasmas decrease with increasing ion energy, as do most of the charge-exchange cross sections above 10 keV amu^{-1}, ENA spectra in this energy range generally decrease even more rapidly with increasing energy than the original ion spectra. The intensity of an ENA flux, however, is derived from the line-of-sight column integral over the space where the ion population overlaps the ambient gas. Reionization of the ENAs along the way modifies the shape and intensity of the ENA spectrum accordingly. For ENAs of heliospheric origin, the +1 ions are the low-energy ACRs at and beyond the termination shock (TS) of the solar wind, and the ambient gas is the neutrals of the local interstellar medium (LISM) (Axford 1972, 1996).

The detection of ENAs of heliospheric origin is of direct interest to the study of cosmic ray propagation in and out of the heliosphere. To date, the cosmic-ray flux beyond the influence of the solar wind can only be inferred by applying models of solar modulation to cosmic-ray fluxes measured along spacecraft trajectories inside the heliosphere (e.g., Cummings & Stone 1996). Since the basic theory of solar modulation was put forward by Parker (1965), three-dimensional solar-wind measurements and ion drift mechanisms have helped to make the models more realistic (Jokipii 1986a). The detection of the ACRs (Garcia-Munoz, Mason, & Simpson 1973; Hovestadt et al. 1973; McDonald et al. 1974; McDonald, Lukasiak, & Webber 1995; Christian, Cummings, & Stone 1995) and the theory of ACRs as pickup ions accelerated in the outer heliosphere

[1] Max-Planck-Institut für Aeronomie, D-37189 Katlenburg-Lindau, Germany.
[2] Department of Physics, University of Arizona, Tucson, AZ 85721
[3] Max-Planck-Institut für Extraterrestrische Physik, D-85740, Garching, Germany.
[4] Physikalisches Institut, University of Bern, CH-3012, Bern, Switzerland.
[5] Department of Physics and Astronomy, University of Maryland, College Park, MD 20742.
[6] ARIAS, Falkenhöhenweg 8, CH-3012, Bern, Switzerland.
[7] EOS, University of New Hampshire, Durham, NH 03824.
[8] Institut für Datenverarbeitungsanlagen, Technische Universität, D-38023, Braunschweig, Germany.
[9] International Space Science Institute, Hallerstr. 6, CH-3012, Bern, Switzerland.
[10] Space Science Center, University of Southern California, Los Angeles, CA 90089.
[11] Institute for Space Physics, Moscow, Russia.
[12] Jet Propulsion Laboratory, Pasadena, CA 91103.

(Fisk, Koslovsky, & Ramaty 1974) or at the TS (Pesses, Jokipii, & Eichler 1981, Jokipii & Giacalone 1996) have provided a self-consistent check between models of diffusive acceleration at the termination shock and three-dimensional solar modulation (Jokipii 1986b). Because ENAs move in ballistic trajectories from their origins, the detection of ENAs of heliospheric origin at the orbit of Earth conveniently yields a direct estimate of the ACR spectra and anisotropy in the regions beyond the termination shock. Such an estimate would give an independent check on the models of acceleration and solar modulation.

We report the first results from the HSTOF sensor of CELIAS on *SOHO*, which is the first instrument flown with the capability and intent to detect ENAs of interplanetary and heliospheric origin. Orbiting the Sun about the Lagrangian point L1, HSTOF completes a 360° scan of the ecliptic in the course of 1 yr. Between 1996 February 13 and 1997 August 31, near solar minimum, HSTOF scanned the apex of the heliosphere once, (254°, 6°) in heliocentric ecliptic longitude and latitude, respectively (Geiss & Witte 1996), and the antiapex of the heliosphere twice. The intensity and time profile of the energetic hydrogen atom (EHA) flux observed during quiet times in this period, translated into a directional distribution of EHAs, support the belief that EHAs coming from the termination shock and beyond have been detected for the first time.

2. INSTRUMENTATION

HSTOF is one of two sections of the Suprathermal Time-of-Flight instrument (STOF) of CELIAS; the other section is also called STOF. A detailed description of the instrument is given by Hovestadt et al. (1995). The Max-Planck Institut für Extraterrestrische Physik was the prime hardware institution for STOF; Universität Bern provided the ion deflection system, and Technische Universität Braunschweig provided the data-processing unit.

The HSTOF section has its boresight set at 37° west of the Sun-*SOHO* line and scans the ecliptic with a field of view (FOV) ± 2° in and ±17° off the ecliptic about its boresight as *SOHO* orbits the Sun. Figure 1 illustrates the viewing geometry of HSTOF in the ecliptic, as the Sun moves through the LISM.

HSTOF identifies the mass and energy of each incident energetic particle by its speed measured by a time-of-flight (TOF) unit and the residual energy deposited in a pixellated solid-state detector (PSSD). In front of the TOF unit is a flat-field electrostatic energy/charge (E/Q) filter that cuts off ions of $E/Q < 80$ keV e^{-1}.

Between the E/Q filter and the TOF unit is a layered foil of Si-Lexan-C (of thicknesses 28, 31, and 5 nm, respectively), supported by a Ni grid with 82% transmission. The foil suppresses the incident photons, most importantly the H Lyα, by 10^{-3}. It also provides the secondary electrons, produced by the passage of an incident particle, to generate the start pulse for TOF analysis. The particle passes through the TOF unit and reaches the PSSD, which has an energy resolution of about 12 keV. HSTOF has an energy threshold of 55 keV for protons (established by the layered foil, the Al window of the PSSD, and the electronic threshold) and an energy ceiling of 80 MeV for heavy ions. The stop signals for TOF are generated by secondary electrons emitted from the front Al window of the PSSD upon particle impact. The secondary electrons from the rear of the foil and the front of the PSSD are accelerated and deflected by an electrostatic
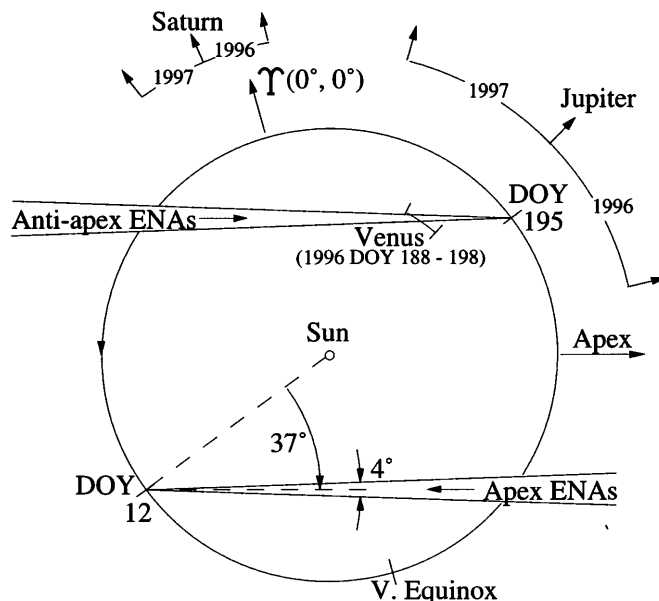

FIG. 1.—Viewing geometry of HSTOF in the ecliptic seen from the north pole. HSTOF's FOV (±2° in and ±17° off the ecliptic) points 37° west of the Sun-*SOHO* line. The FOV moves with the day-of-year (DOY) as *SOHO* orbits the Sun, thus sweeping a ±17° wide belt about the ecliptic, including the apex and antiapex of the heliosphere, once a year. Features in the time profile of the detected ENA flux provide a measure of the ENA anisotropy. The close passing of Venus in 1996 and the angular positions of Jupiter and Saturn over the span of 1996 and 1997 are indicated.

mirror onto the respective microchannel plates (MCPs). The particles are detected as triple coincidence events: start and stop of the TOF and the energy signal from the PSSD. The detection efficiency depends on the energetic particle energy loss and scattering in the foil and PSSD Al window and dead layer. The efficiency of the TOF unit is 0.05 at 55 keV and 0.03 at 500 keV. The total geometrical factor of HSTOF for an isotropic flux is 0.22 cm² sr.

HSTOF's E/Q filter consists of a stack of six parallel plates, each 0.45 cm apart. Serration on the plates suppresses scattered particles from entering the TOF unit. The voltages of $+1.26$ kV and -1.26 kV applied to the adjacent plates determine the E/Q cutoff of the filter. The ability of the HSTOF flat-plate filter to effectively suppress ions <89 keV e^{-1} is indicated by the ion transmission based on preflight calibration (Fig. 2a, *filled circles*). The ion transmission curve is shown from preflight calibration with ions incident from all azimuthal angles α, and 0° in angle β, the complement of polar angle. The vertical error bars are based on 3 σ in Poisson statistics, and the horizontal error bars are estimated from the resolution (A/D converter ±1/2 bit) of the high-voltage housekeeping readout. Computer Monte Carlo simulations under the same conditions, including scattering and transmission of particles in the layered foil (Ho et al. 1996), produced a series of points (Fig. 2a, *open circles*) at different energies that match well with the calibration points. For the ion transmission at 80 keV, the result of the Monte Carlo simulation is 4×10^{-3}, dropping further for particle energies <80 keV to values of $<1 \times 10^{-3}$. The condition $\beta = 0°$ is expected to yield an ion transmission higher than the actual value, because ions incident at $\beta = 0°$ have the minimum path length in the electrostatic field. When the full range of β is included, as in flight, the ion transmission is expected to be lower than that
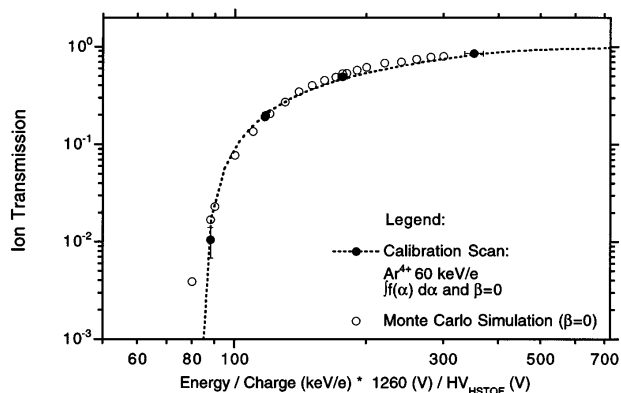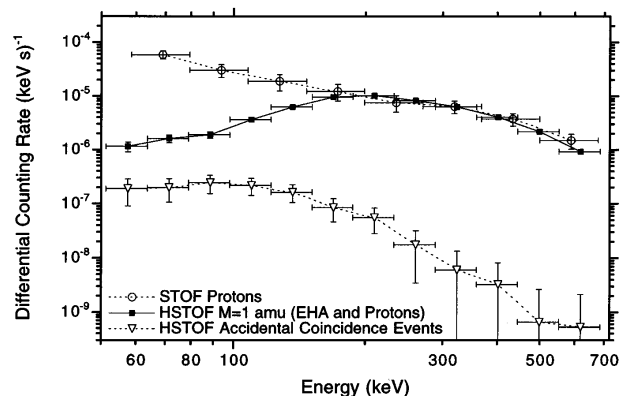
FIG. 2a

FIG. 2b

FIG. 2.—(a) HSTOF's transmission factor for ions as a function of the ion energy/charge (E/Q) for a given filter high-voltage setting (± 1260 V). The measured transmission (*filled circles*) is compared to a Monte Carlo simulation (*open circles*), both for $\beta = 0°$. Simulation points for E/Q below 80 keV e^{-1} lie well below 10^{-3}. Errors are given in 3 σ Poisson statistics. (b) Differential counting rates for $M = 1$ amu as a function of the particle energy measured by STOF and HSTOF between 1996 February 13 and 1997 August 31, including periods of high levels of solar and interplanetary protons fluxes. The differential flux measured by STOF (*open circles*) is normalized, while that of HSTOF (*filled squares*) and the accidental coincidence events (*open triangles*) are uncorrected. The deviation between the rates observed by STOF and HSTOF in the energy interval 80–400 keV is due to the action of the ion-repelling E/Q filter of HSTOF. The HSTOF rates at energies <80 keV are due to EHAs. The background rate is obtained from accidental-coincidence events in equivalent energy channels. All data points carry a $\pm 3 \sigma$ statistical uncertainty.

at $\beta = 0°$ alone. The actual cutoff (ion transmission <1%) should be closer to 100 keV e^{-1}. Since neutral particles incident within the FOV of ($\pm 2°$, $\pm 17°$) pass the HSTOF E/Q filter unimpeded, it is safe to take 80 keV e^{-1} as the cutoff for separating energetic hydrogen atoms (EHAs) from protons.

The STOF section also uses TOF and PSSD to determine the mass and energy of the incident particles. STOF differs from HSTOF, however, in two main features. STOF has a curved-plate E/Q analyzer, and its 3° × 17° FOV points only 7° west of the Sun-*SOHO* line. STOF measures energetic ions from protons to Fe in the E/Q range of 35–630 keV e^{-1}, in 30 logarithmic spaced steps with an E/Q resolution of $\Delta(E/Q)/(E/Q) = 0.11$. The geometrical factor is 0.05 cm² sr. Because of the E/Q stepping and the smaller geometrical factor, the sensitivity of STOF is about 0.008 that of HSTOF for energetic protons. STOF is more sensi-

tive to scattered ultraviolet light than expected, and therefore exhibits a relatively high background from accidental coincidence rates. The curved-plate E/Q analyzer, however, makes STOF insensitive to neutral particles.

3. OBSERVATIONS

STOF's insensitivity to neutral particles and HSTOF's ability to effectively suppress ions <80 keV e^{-1} work together for the detection and identification of energetic neutral atoms (ENAs) with energies <80 keV e^{-1}. We shall concentrate on particles of mass $M = 1$ amu, i.e., protons and energetic hydrogen atoms (EHAs), or H events, henceforth.

Figure 2b shows the energy distributions for H events, as collected by HSTOF and STOF between 1996 February 13 and 1997 August 31. These data contain solar energetic particles (SEP), energetic particles in corotating interaction regions (CIR), coronal mass ejecta (CME), and quiet times (QT). The rates measured by STOF (Fig. 2b, *open circles*) have been normalized, taking into account the geometrical factor, duty cycle, and sensitivity of STOF relative to HSTOF. As expected, this distribution decreases with increasing particle energy, typical for solar or interplanetary protons (STOF is only sensitive to charged particles).

The energy distribution of H events measured by HSTOF (Fig. 2b, *filled squares*) clearly decreases with respect to that of proton events measured by STOF (*open circles*) as the energy decreases below 200 keV. This feature is understood in terms of HSTOF's ion transmission, shown in Figure 2a: low-energy protons are suppressed by the E/Q filter. Instead of continuing to drop with decreasing energy, the differential counting rate of H events at lower energies levels at 1×10^{-6} (keV s)$^{-1}$. We attribute the H events observed between 55 and 80 keV mainly to EHAs. EHAs of energies below 55 keV are cut off by HSTOF's energy threshold.

It is still possible, however, that the differential counting rates in the 55–80 keV interval could be due to instrument background. To estimate the background, we examine the pulse-height analysis flight data, an example of which is shown in Figure 3a. True events due to real particles congregate along well-defined tracks in the plane of residual-energy channels versus TOF channels, i.e., the T-E plane, according to their respective masses (Fig. 3b). Events scattered throughout the T-E plane, where no real particle tracks are expected, are accidental coincidence events. Those accidental events occurring along the well-defined tracks for real particles, and hence mingled with the real events, constitute the background that must be subtracted. To estimate the background among the H events, we displace the $M = 1$ track, with its track width, by a block of TOF channels (500 channels, say, as in Fig. 3c) into the region of the T-E plane, where no real particles are expected. Since the accidental events are observed to be randomly distributed among TOF channels, all events falling within any energy channel intervals on this displaced track provide a true measure of the background in the same energy channel intervals on the real $M = 1$ track. Background rates obtained thus in equivalent incident energy intervals are shown as open triangles in Figure 2b. These rates give an integrated background rate of about 5×10^{-6} s^{-1} in the 55–80 keV incident energy interval. This rate is about 3 times that obtained by a Monte Carlo simulation of the accidental triple coincidence rate caused by an isotropic
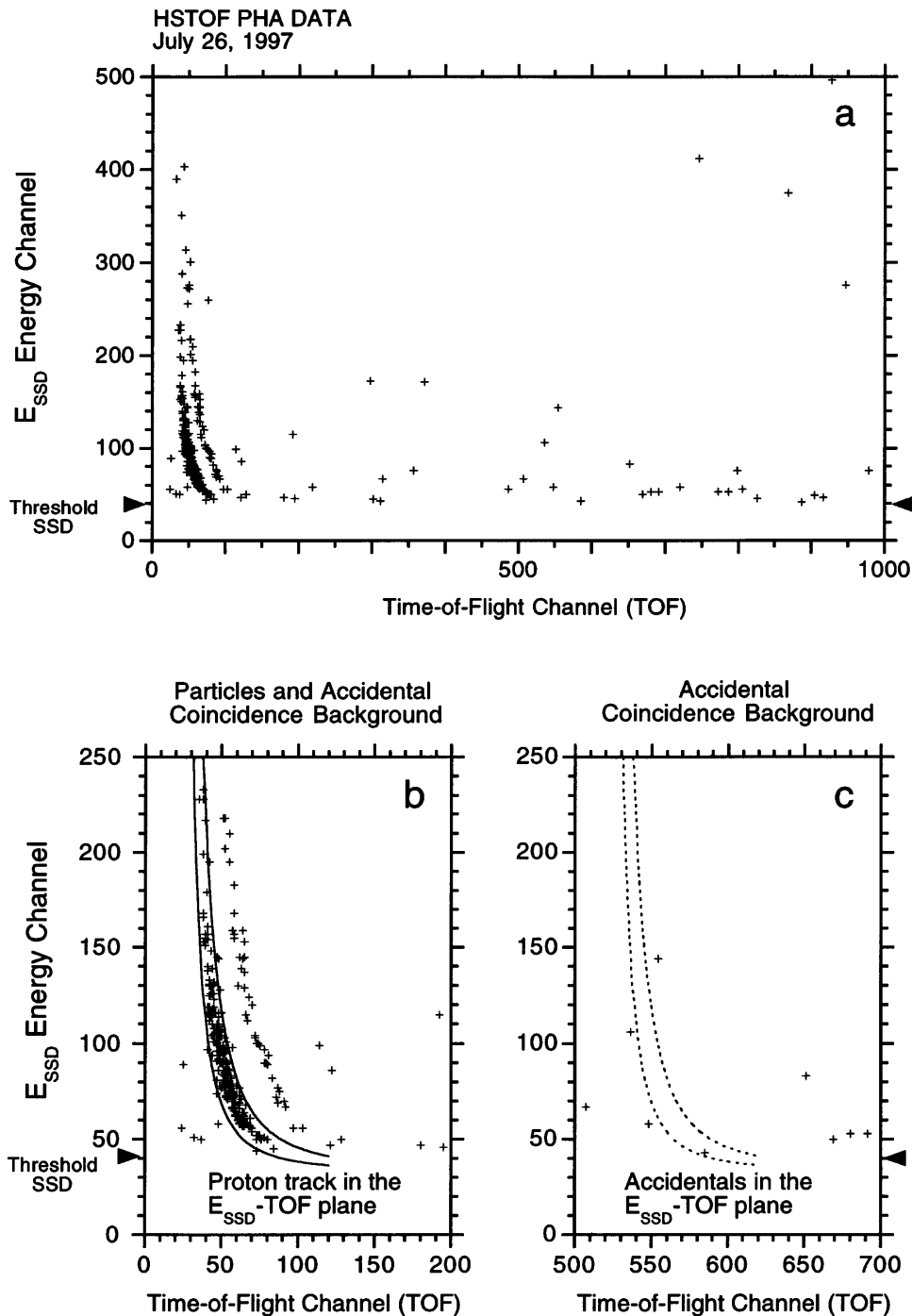
HSTOF PHA DATA
July 26, 1997

FIG. 3.—Distribution of real particle events and accidental-coincidence events in the energy vs. TOF plane (T-E plane). (a) An example of pulse height analysis (PHA) flight data is plotted in the T-E plane. The H and He events and the accidental coincidence events are clearly distinguishable. (b) According to their masses, particle events congregate along well-defined tracks in the T-E plane. Tracks of real particle events can only be detected in the first half-section of the time-of-flight range. (c) The accidental coincidence events scatter uniformly throughout the entire TOF regime and fall randomly within the tracks.

flux of higher energy cosmic-ray protons and electrons, which would deposit similar amounts of energy in the PSSD along shorter paths in traversing the detector. This comparison suggests that the flight data provide a reliable upper limit measurement of the background. The H events in the 55–80 keV interval are significantly above this accidental coincidence background.

To separate the EHAs of heliosheath origin from those of solar and interplanetary origin, it is necessary to exclude all

EHAs detected during known solar and interplanetary particle events. The number of STOF proton events per day in the energy interval 55–600 keV from 1996 February 13 to 1997 August 31 are plotted in Figure 4a. The number of H events (EHAs and protons) per day detected in the same energy and time interval by HSTOF are plotted in Figure 4b. The peaks include energetic particle events such as CMEs, SEPs, and CIRs; some events having 27 day periodicity, due to solar rotation, are clearly discernible. The much

lower sensitivity of STOF compared to HSTOF is clearly visible. Between the days of high HSTOF fluxes are the quiet times (QT), defined as intervals lasting more than 5 days with no more than 12 particles each day detected by HSTOF (Fig. 4b). Possible proton contamination of the long-term EHA analysis is further suppressed by analyzing EHA events during QT only.

The energy distribution of the H events from the QT (285 days, 31 periods) is shown in Figure 5a (*filled squares*). The distribution of the background due to accidental-coincidence events in the equivalent *E*-channels is also shown (*open triangles*), both with ± 3 σ error bars. The EHA event rate during the QT is significantly above the background. The STOF proton observations, normalized as in Figure 2b, are shown for comparison (*open circles*). As the 3 σ error of the STOF proton observation has the magnitude of the observed proton flux, the STOF observation during QT corresponds to the upper limit of the QT proton flux. The QT energetic proton flux is much reduced, as expected, but the EHA/proton ratio is clearly enhanced during the QT compared to that in Figure 2b. The valid understanding of the ion transmission of HSTOF based on calibration and simulation, the clear comparison between the measured $M = 1$ amu fluxes by HSTOF and STOF, the
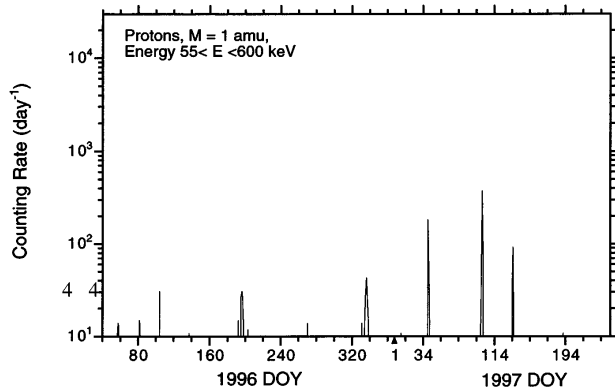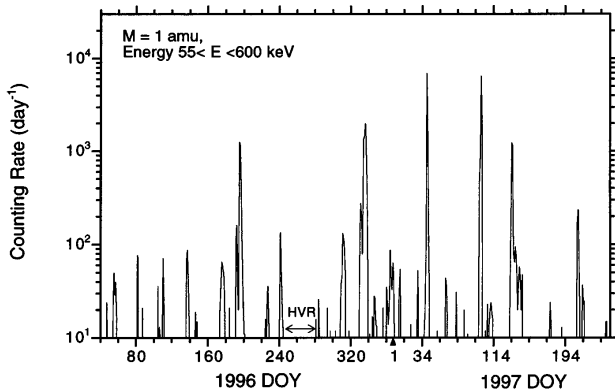

FIG. 4a

FIG. 4b

FIG. 4.—(a) Daily counting rate for protons in the energy interval 55–600 keV measured by STOF, between 1996 February 13 and 1997 August 31. The sensitivity of STOF is about 0.008 that of HSTOF. (b) Daily counting rate for $M = 1$ amu measured by HSTOF in the same energy range and time period. All elevated rates are associated with solar or interplanetary events, some showing obvious 27 day recurrence. Days with counting rates <12 day^{-1} are considered quiet times (QTs). In the interval marked HVR, the high voltage on the HSTOF E/Q filter was reduced, and ions could not be discriminated from EHAs.
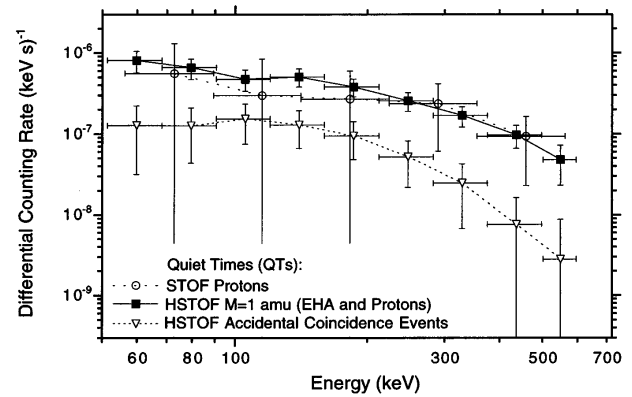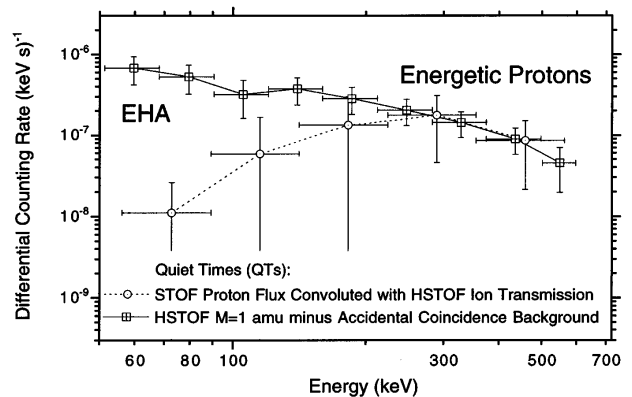

FIG. 5a

FIG. 5b

FIG. 5.—(a) Differential counting rate for $M = 1$ amu as function of particle energy measured by HSTOF during QTs between 1996 February 13 and 1997 August 31 (*filled squares*). The distribution of the accidental coincidence events in equivalent energy channels (*open triangles*) and the STOF proton observations (*open circles*) are shown for comparison. The STOF 3 σ (Poisson statistics) error bars are much larger than the ones on the HSTOF observations, because of the low STOF counting rate during QT. Therefore, the STOF observations constitute the upper limit on the interplanetary proton flux during QT. The HSTOF EHA event rate during the QT is significantly above the accidental coincidence events. (b) Differential counting rate of the HSTOF EHA and proton flux and the STOF proton flux convoluted with the HSTOF ion transmission (error magnitude is about the same as for the corresponding open circles in (a), since the statistical error dominates the uncertainty in the ion transmission function). The regions for EHA and energetic proton detection by HSTOF are well separated.

safe estimate of the background, and the careful choice of the QT together give us confidence to claim that the $M = 1$ amu event rates between 55 and 80 keV shown in Figure 5b are due to EHAs in that energy interval. After folding in the geometrical factor and detection efficiency, the mean EHA flux in this energy interval is $(8.0 \pm 0.8) \times 10^{-5}$ (cm^2 sr s keV)$^{-1}$. The detection threshold as derived from the accidental coincidence counts $+3$ σ is 2×10^{-5} (cm^2 sr s keV)$^{-1}$.

4. RESULTS AND DISCUSSION

After examining the instrument behavior and observational conditions, the data analyzed strongly suggest that energetic hydrogen atoms (EHAs) have been detected at L1, under quiet interplanetary conditions, between 1996 February 13 and 1997 August 31, near solar minimum. The observed EHA rate is shown as a function of the day-of-

year (DOY) in Figure 6a (*filled squares*). The EHA flux varies between 0.2 and 3.4×10^{-4} $(cm^2 \, sr \, s \, keV)^{-1}$. The lowest values are comparable to the HSTOF detection threshold. The flux, however, is significantly peaked around 1996 DOY 130 and DOY 206 as well as 1997 DOY 195. While the first peak is rather isolated, the other two peaks are spread over about 15 days and occur around the same DOY. For comparison, we plotted the accidental coincidence rate or background (Fig. 6a, *open triangles*) and the energetic proton flux (*solid crosses*) for the same QT periods. The mean QT energetic proton flux in the energy range from 400 to 600 keV is $1.5 \pm 0.8 \times 10^{-5}$ $(cm^2 \, sr \, s \, keV)^{-1}$. The EHA flux is not correlated with the background or the energetic protons (correlation coefficient $R = 0.28$ or 0.03, respectively). In interpreting the data, it is important to note that only QT fluxes were selected, and that intense particle events are excluded from this analysis.

We now try to identify the most likely source of this EHA

flux and its immediate implications. To guide us in this endeavor, the look directions of HSTOF in heliocentric ecliptic longitudes are indicated at the top of Figure 6a.

1. *Planetary EHAs.*—HSTOF's viewing direction (Fig. 1) precludes EHAs from Earth. During the period around 1997 DOY 71, Jovian EHAs could have reached HSTOF, at a distance of 2.4×10^3 Jovian radii, and similarly for Saturn around 1996 DOY 120. In fact, no distinct feature is seen during these planetary crossing periods (Fig. 6a). The absence of signals from Jupiter and Saturn is as expected, based on the fluxes observed prior to the Voyager fly-bys (Kirsch et al. 1981a, 1981b). Venus crossed HSTOF's field of view between 1996 DOY 188 and DOY 196 at distances from 5.6 to 6.4×10^7 km (Fig. 1), when the interplanetary proton flux was high (Fig. 4b). Therefore, that period was omitted from the analysis. In short, none of the known ENA-producing planets contributed the EHA events analyzed and reported here.

2. *Interplanetary EHAs.*—Possible sources of interplanetary EHAs are energetic protons in solar particle events, transient shocks, corotating interaction regions, or merging interaction regions (H1; H2; Roelof 1992). These proton fluxes would be associated with known solar energetic particle or interplanetary events (Fig. 4b). Consequently, the interplanetary EHA fluxes would also have distinctive directional distributions and characteristic times or spatial dimensions; e.g., due to the spiral structure of CIRs, EHAs from a CIR should be seen at 1 AU during and a few days after that CIR's passing about every 27 days. The time profile shown in Figure 6a does not fit any such features. H1 also estimated the EHA flux from the quiet-time interplanetary protons, which is about 2 orders of magnitude below the observed flux. Also shown in Figure 6a is the time profile of 400–600 keV proton flux during the same QT (*bottom panel, solid cross*). The lack of correlation between the EHAs and these high-energy protons (correlation coefficient of 0.03) further suggests that the EHA flux between 55 and 80 keV is not of local or interplanetary origin. Our intentional exclusion of all periods with elevated levels of interplanetary proton flux and the lack of expected temporal features suggest that no discernible interplanetary EHA flux contributed to the EHA events analyzed and reported here.

3. *Heliospheric EHAs.*—By the logic of elimination, we could conclude that the heliospheric EHAs are the most likely candidate for the observed QT EHA events. The reappearance of the maximum flux coming from the antiapex in two consecutive years especially favors this identification. Heliospheric EHAs are produced when low-energy ACR protons at and beyond the TS exchange charge with the neutral atoms of the LISM. The relatively quiet Sun during this solar minimum is especially favorable for observing heliospheric EHAs, and the exclusion of all periods with elevated proton flux also enhances the chance of detecting heliospheric EHAs. The directional and energy distributions of heliospheric EHA flux between 10 keV and 1 MeV have been estimated using the ACR protons accelerated at the TS as the source (H1; H2). A much improved calculation, including the convection and diffusion of the ACR in the heliosheath region bounded by the TS and the heliopause, indicates a strong anisotropy in the EHA flux in the antiapex direction of the heliotail (CGM). The heliospheric EHA flux depends on the ACR spectrum at the TS
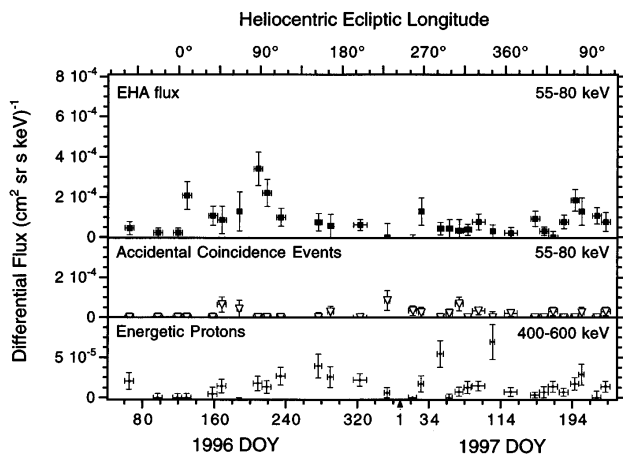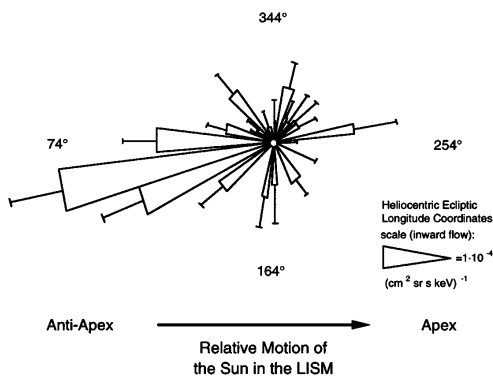

FIG. 6a

FIG. 6b

FIG. 6.—(a) Differential flux of QT 55–80 keV EHA as observed by HSTOF after background subtraction (*upper panel, filled squares*). The look direction of HSTOF in heliocentric ecliptic longitude is indicated at the top of the panel. For comparison, the background level (*middle panel, open triangles*) and the energetic proton fluxes (*bottom panel, solid crosses*) are plotted for the same quiet times. The EHA flux correlates neither with the background nor with the energetic protons fluxes. Errors are given in 1 σ Poisson statistics. The enhanced EHA flux observed near 1996 DOY 200 reappeared 1 yr later, at a lower level. (b) Anisotropy of QT 55–80 keV EHA flux (1996 DOY 203 to 1997 DOY 200). Translating the day-of-year (DOY) of observation by HSTOF into the look direction of HSTOF, as indicated by Fig. 1, the time profile of the EHA flux shown in Fig. 5a is converted into the angular distribution in the ecliptic plane. The peak of the distribution is in the general direction of the heliotail or the antiapex (heliocentric ecliptic longitude 74°).

and the thickness of the heliosheath; H1 and H2 used the ACR flux at TS of Jokipii (1986b), and CGM that of Stone, Cummings, & Webber (1995); the two models yielded comparable EHA fluxes of about 10^{-4} $(cm^2 \, sr \, s \, keV)^{-1}$ at 60 keV, which matches our observation. Since our understanding of the heliosphere suggests longer temporal and larger spatial features in the heliospheric EHA fluxes, in contrast to those of the interplanetary EHAs, we also look for signatures in the time profile of the EHA flux. Furthermore, as *SOHO* orbits the Sun about L1 (Fig. 1), the slowly varying time profile of the heliospheric EHA flux (Fig. 6a) can be translated into a directional distribution (Fig. 6b). Both the long-term flux level and the deduced directional distribution, i.e., the recurrence of a statistically significant enhancement in the EHA flux near DOY 200 1 yr apart that translates into an anisotropy coming from the heliotail, suggest that the EHAs detected best fit the expected features of heliospheric EHAs, especially that of CGM. According to CGM's axial-symmetric model, a maximum EHA flux occurs at longitude $l = 74°$, or to be observed by HSTOF on DOY 195 each year. This is indeed the case in 1997. In 1996, however, the period around DOY 195 was excluded from QT analysis because of an energetic solar particle event (Fig. 4). A large flux of EHA was detected around 1996 DOY 206 or around $l = 85°$, still in the general heliotail direction.

Identifying heliospheric EHAs with an anisotropy in the heliotail as the most likely candidate for our observed EHAs leaves some questions and implications for careful consideration in future work.

(i) *The high flux around 1996 DOY 130.*—This seemingly isolated peak begs for an explanation, or it suggests some structure in the heliotail. No associations with solar or interplanetary energetic particle events have been found (Fig. 4). The search for an answer must continue.

(ii) *The difference between the flux level near 1996 DOY 200 and that in 1997.*—In view of the fact that the boundary of the heliosphere need not be steady state with an axial symmetry, a change in the heliospheric EHA flux level in 1 yr could be due to solar conditions or any "wagging" of the heliotail. The implications in the amount of change should be studied.

(iii) *The direction of the anisotropy.*—The possible angular deviation from axial symmetry and the implied magnetic field orientation in the LISM warrant further investigation.

5. CONCLUSION

The instrument HSTOF of CELIAS on *SOHO* at L1 has detected energetic hydrogen atoms (EHAs) in the energy interval 55–80 keV over a 20 month interval in 1996 and 1997. The EHA flux, detected under quiet interplanetary conditions, is most likely coming from the heliosheath, thus constituting the first detection of energetic neutral atoms coming from beyond the termination shock of the solar wind. The detection and modeling of heliospheric EHAs provides a link between those of pickup ions and anomalous cosmic rays (ACR) in probing the heliosphere. The use of HSTOF data and refined modeling for these studies will continue, in particular extending to energetic He atoms. Our investigation should also define the design parameters for the next generation of energetic neutral atom instruments for a more comprehensive study of the heliosphere. More immediately, we look forward to the promise held by INCA (Mitchell et al. 1996), an energetic neutral atom instrument on the *Cassini* mission to Saturn with a larger geometrical factor and lower energy threshold than HSTOF, provided that cruise-mode science will be conducted.

REFERENCES

Axford, W. I. 1972, in Solar Wind, ed. C. P. Sonnet, P. J. Coleman, Jr., & J. M. Wilcox (NASA SP-308), 609
Axford, W. I. 1996, Space Sci. Rev., 78, 9
Christian, E. R., Cummings, A. C., & Stone, E. C. 1995, ApJ, 446, L105
Cummings, A. C., & Stone, E. C. 1996, Space Sci. Rev., 78, 117
Czechowski, A., Grzedzielski, S., & Mostafa, I. 1995, A&A, 297, 892 (CGM)
Fisk, L. A., Koslovsky, B., & Ramaty, R. 1974, ApJ, 190, L35
Fleck, B., Domingo, V., & Poland, A. I., ed. 1995, The *SOHO* Mission (Dordrecht: Kluwer)
Garcia-Munoz, M., Mason, G. M., & Simpson, J. A. 1973, ApJ, 182, L81
Geiss, J., & Witte, M. 1996, Space Sci. Rev., 78, 229
Ho, G. C., Hamilton, D. C., Adrian, M. L., Pollock, C. J., Moore, T. E., Magi, B. I., & Hsieh, K. C. 1997, NIM (B), submitted
Hovestadt, D., Vollmer, O., Gloeckler, G., & Fan, C. Y. 1973, Phys. Rev. Lett., 31, 650
Hovestadt, D. et al. 1995, Sol. Phys., 162, 441
Hsieh, K. C., & Gruntman, M. A. 1993, Adv. Space Res., 13 (6), 131
Hsieh, K. C., Shih, K. L., Jokipii, J. R., & Grzedzielski, S. 1992a, ApJ, 393, 756 (H1)
Hsieh, K. C., Shih, K. L., Jokipii, J. R., & Gruntman, M. A. 1992b, in Solar Wind Seven, ed. E. Marsch & R. Schwenn (Oxford: Pergamon), 365 (H2)
Jokipii, J. R. 1986a, in The Sun and the Heliosphere in Three Dimensions, ed. R. G. Marsden (Dordrecht: Reidel), 375
Jokipii, J. R. 1986b, J. Geophys. Res., 91, 2929
Jokipii, J. R., & Giacalone, J. 1996, Space Sci. Rev., 78, 137
Kirsch, E., Krimigis, S. M., Ip, W.-H., & Gloeckler, G. 1981a, Nature, 292, 718
Kirsch, E., Krimigis, S. M., Kohl, J. W., & Keath, E. P. 1981b, Phys. Rev. Lett., 8, 169
McDonald, F. B., Lukasiak, A., & Webber, W. R. 1995, ApJ, 446, L101
McDonald, F. B., Teegarden, B. J., Trainor, J. H., & Webber, W. R. 1974, ApJ, 185, L105
Mitchell, D. G., et al. 1996, Proc. SPIE, 2803, 154
Parker, E. N. 1965, Planet. Space Sci., 13, 9
Pesses, M. E., Jokipii, J. R., & Eichler, D. 1981, ApJ, 246, L85
Roelof, E. C. 1992, in Solar Wind Seven, ed. E. Marsch & R. Schwenn (Oxford: Pergamon), 385
Stone, E. C., Cummings, A. C., & Webber, W. R. 1995, Geophys. Res. J., 101(A5), 11017